JOC Article

Diboron and Triboron Compounds Based on Linear and Star-Shaped Conjugated Ligands with 8-Hydroxyquinolate Functionality: Impact of Intermolecular Interaction and Boron Coordination on Luminescence

Yi Cui and Suning Wang*

Department of Chemistry, Queen's University, Kingston, Ontario, K7L 3N6 Canada

wangs@chem.queensu.ca

Received April 21, 2006

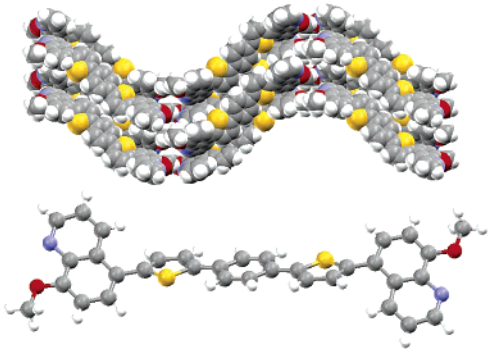

New 8-R-quinoline functionalized linear and star-shaped conjugated molecules have been synthesized using Suzuki−Miyaura coupling methods (R = MeO, **L1**−**L5**; R = CH_3OCH_2O, **L1′**−**L5′**). When treated with HCl, **L1′**−**L5′** are converted readily to the corresponding 8-hydroxyquinoline compounds **L**(OH)-**1**−**L**(OH)**5** which react readily with BPh_3 in refluxing THF to produce the corresponding polyboron chelate compounds **B1**−**B5** in good yields. **L1**−**L5** and **B1**−**B5** display similar thermal stability with T_d at ∼300 °C. Experimental and molecular orbital calculation results showed that the chelation by boron stabilizes the LUMO level of the ligand and narrows the HOMO−LUMO gap, resulting in the blue emission of the ligands and the green or orange emission of the boron compounds. Crystal structures of **L1**, **L3**, and **L5** showed that these molecules have layered arrangements in the solid state with significant intermolecular $\pi-\pi$ interactions. The linear diboron **B5** displays concentration and temperature-dependent emission in solution, attributable to intermolecular interactions. The properties of a monoboron compound BPh_2(5-Ph-8-MeO-q) (**B0**) and its corresponding free ligand **L0** were investigated and compared to the closely related diboron compound **B1** and the ligand **L1**, which revealed that the increase of the number of chromophores linked by an aromatic group has a significant impact on thermal stability and the HOMO and LUMO energy levels.

Introduction

8-Hydroxyquinoline and its derivatives have attracted much research interest since the breakthrough report on organic light emitting devices (OLEDs) based on a chelate complex Alq_3 (q = 8-hydroxyquinolate) by Tang and VanSlyke.[1] Inspired by the successful applications of Alq_3 in OLEDs, much research efforts have been dedicated to the development of new derivative molecules based on 8-hydroxyquinoline. The bulk of the new derivative molecules are small aluminum chelate compounds with the general formula of Alq'_3 where q′ is a 8-hydroxyquinolate analogue that contains various substituent groups.[2−7] Other 8-hydroxyquinoline metal chelate compounds that have been investigated include Liq,[8] Mq_2 where M = Be, Mg, and Zn,[9]

(1) Tang, C. W.; VanSlyke, S. A. *Appl. Phys. Lett.* **1987**, *51*, 913.

(2) (a) Jang, H.; Do, L.-M.; Kim, Y.; Gon Kim, J.; Zyung, T.; Do, Y. *Synth. Met.* **2001**, *121*, 1669. (b) Jang, H.; Do, L.-M.; Kim, Y.; Zyung, T.; Do, Y. *Synth. Met.* **2001**, *121*, 1667.

(3) (a) Matsumura, M.; Akai. T. *Jpn. J. Appl. Phys.* **1996** *35*, 5357. (b) Burrows, P. E.; Shen, Z.; Bulovic, V.; McCarty, D. M.; Forrest, S. R.; Cronin, J. A.; Thompson, M. E. *J. Appl. Phys.* **1996**, *79*, 7991.

10.1021/jo060841+ CCC: $33.50
Published on Web 07/26/2006

and Mq_3 where M = Ga, In, Sc.[10] We reported a series of monoboron compounds with the general formula of BPh_2q' and BAr_2q' where q′ is either 8-hydroxyquinolate or its derivative and Ar is an aryl group other than phenyl.[11] The key feature of the previously investigated hydroxyquinolate derivative compounds is the presence of *N*,*O*-chelation with a metal ion or a main group element because such chelation is critical for the chromophore to achieve a high luminescent efficiency and a high thermal stability (e.g., Alq_3 versus the free 8-hydroxyquinoline). In addition to small molecules, a number of polymer compounds that contain covalently attached boron 8-hydroxyquinolate chelate units or aluminum 8-hydroxyquinolate chelate units have been reported with the aim to enhance the solution processing ability and the thermal stability of the materials.[12] To improve the properties of small molecule based materials, we have extended our investigation on 8-hydroxyquinolate boron chelate compounds to di- and triboron compounds using linear and star-shaped ligands that contain multiple quinolate groups. In addition to enhanced thermal stability, the new polyboron compounds provide an unique opportunity for the investigation of intermolecular interactions and their impact on physical and photophysical properties because of the highly anisotropic shape of linear and star-shaped molecules. Furthermore, the presence of multiboron centers and multiple chromophores in the linear and star-shaped molecules allows us to examine the possible cooperative electronic effects. Five new linear and star-shaped ligands and their corresponding boron chelate compounds have been achieved. For comparison purposes, a monoboron compound BPh_2(5-Ph-8-MeO-q) that is closely related to one of the linear diboron compounds has also been synthesized. The synthetic details and the properties of these new molecules are reported herein.

Results and Discussion

Syntheses

The first set of new ligands synthesized are derivatives of 8-methoxyquinoline or 8-methoxy-2-methylquinoline with a linear or star-shaped conjugated core, 4,4′-di[5″-(8″-methoxyquinoline)]biphenyl (**L1**), 4, 4′-di[5″-(8″-methoxy-2″-methylquinoline)]biphenyl (**L2**), 1, 3, 5-tri[*p*-5″-(8″-methoxyquinoline)phenyl]benzene (**L3**), 2, 4, 6-tri[*p*-5″-(8″-methoxyquinoline)-phenyl]-1,3.5-triazine (**L4**) and 4-di(2′-thienyl-5′-(8-methoxyquinoline)-benzene (**L5**). The synthetic methods employed for **L1**−**L5** are Suzuki coupling reactions involving the appropriate boronic acid of the central core and 5-bromo-8-methoxyquinoline or 5-bromo-8-methoxy-2-methylquinoline as shown in Scheme 1. The boronic acids for **L1**−**L4** were synthesized from the corresponding parent bromo compounds according to modified known procedures.[14] The key intermediates 1,3,5,-tri-(*p*-bromophenyl)benzene and 1,3,5,-tri(*p*-bromophenyl)triazine for **L3** and **L4** were prepared by trimerization of 4-bromobenzonitrile and 4-bromoacetophenone, respectively, using previously reported procedures.[21] The synthesis of **L5** involved the preparation of the intermediate, 4-di(2-thienyl)benzene and its conversion to the boronic acid using a literature procedure.[15] In principle, the Suzuki coupling reactions for **L1**−**L5** could also be accomplished by the reaction of 8-methoxyquinoline-5-boronic acid with the appropriate bromo derivative of the central core. However, the conversion from 5-bromo-8-methoxyquinoline to its boronic acid was not satisfactory and as a result, this approach was abandoned. For comparison purposes, the monocompound 5-phenyl-8-MeO-quinoline (Ph-8-MeO-q, **L0**) was also synthesized. The **L0** molecule is exactly one-half of **L1**.

Attempts were made to convert the 8-methoxy group to a 8-hydroxy group in ligands **L1**−**L5** by using BBr_3 or HCl to produce the corresponding **L**(OH)**1**−**L**(OH)**5** ligands. However, surprisingly, the yield of the demethylation reaction was low, despite many trials. To improve the yield of the demethylation reaction, we synthesized the second set of ligands **L1′**−**L5′** where the 8-methoxy group is replaced with a CH_3OCH_2O (MOMO) group to make it a better leaving group. Using the same synthetic procedures as for ligands **L1**−**L5**, ligands **L1′**−**L5′** were obtained in good yields (62−71%). In contrast to **L1**−**L5**, the MOM group in **L1′**−**L5′** can be removed readily with methanolic HCl to afford excellent yields (85−92%) of the 8-hydroxy quinoline ligands **L**(OH)**1**−**L**(OH)**5**. Unlike the methyl or the MOM protected ligands **L1**−**L5** and **L1′**−**L5′** which are moderately soluble in solvents such as CH_2Cl_2 or THF, **L**(OH)**1**−**L**(OH)**5** have a poor solubility in CH_2Cl_2 or THF and are slightly soluble in strong polar solvents such as

(4) (a) Sapochak, L. S.; Padmaperuma, A.; Washton, N.; Endrino, F.; Schmett, G. T.; Marshall, J.; Fogarty, D.; Burrows, P. E.; Forrest, S. R. *J. Am. Chem. Soc.* **2001**, *123*, 6300. (b) Kido, J.; and Iizumi, Y. *Chem. Lett.* **1997**, *26*, 963. (c) Hamada, Y.; Sano, T.; Fujita, M.; Fujii, T.; Nishio, Y.; Shibata, K. *J. Appl. Phys.* **1993**, *32* L514.

(5) Shoji, E.; Miyatake, K.; Hlil, A. R.; Hay, A. S.; Maindron, T.; Jousseaume, V.; Dodelet, J. P.; Tao, Y.; D'Iorio, M. *J. Polym. Sci. Part A: Polym. Chem.* **2003**, *41*, 3006.

(6) (a) Pohl, R.; Montes, V. A.; Shinar, J.; Anzenbacher, P., Jr. *J. Org. Chem*. **2004**, *69*, 1723. (b) Montes, V. A.; Li, G.; Pohl, R.; Shinar, J.; Anzenbacher, P., Jr. *Adv. Mater*. **2004**, *16*, 2001. (c) Pohl, R.; Anzenbacher, P., Jr. *Org. Lett.* **2003**, *5*, 2769.

(7) (a) Cheng, J.-A.; Chen, C. H. *J. Mater. Chem.* **2005**, *15*, 1179. (b) Cheng, J.-A.; Chen, C. H.; Yang, H. *Chem. Phys. Lett.* **2004**, *397*, 302.

(8) (a) Zheng, X.; Wu, Y.; Sun, R.; Zhu, W.; Jiang, X.; Zhang, Z.; Xu, S.; *Thin Solid Films* **2005**, *478*, 252. (b) Jaafaria, A.; Ouzeaua, V.; Elya, M.; Rodrigueza, F.; Yassar, A,; Aaron, J. J.; Benalloulb, P.; Barthou, C. *Synth. Met.* **2004**, *147*, 175.

(9) (a) Sapochak, L. S.; Benincasa, F. E.; Schofield, R. S.; Baker, J. L.; Riccio, K. K. C.; Fogarty, D.; Kohlmann, H.; Ferris, K. F.; Burrows, P. E. *J. Am. Chem. Soc.* **2002**, *124*, 6119. (b) Donzé, N.; Péchy, P.; Grätzel, M.; Schaer, M.; Zuppiroli, L. *Chem. Phys. Lett.* **1999**, *315*, 405.

(10) Burrows, P. E.; Sapochak, L. S.; McCarty, D. M.; Forrest, S. R.; Thompson, M. E. *Appl. Phys. Lett.* **1994**, *64*, 2718.

(11) (a) Cui, Y.; Liu, Q.-D.; Bai, D.-R.; Jia, W.-L.; Tao, Y.; Wang, S. *Inorg. Chem*. **2005**, *44*, 601. (b).Wu, Q.; Esteghamatian, M.; Hu, N. H.; Popovic, Z.; Enright, G.; Tao, Y.; D'Iorio, M.; Wang, S. *Chem. Mater.* **2000**, *12*, 79.

(12) (a) Iijima, T.; Yamamoto T. *Macromol. Rapid Commun*. **2004**, *25*, 669. (b) Meyers, A.; Weck, M. *Macromolecules*, **2003**, *36*, 1766. (c)-Yamamoto, T.; Yamaguchi, I. *Polym. Bull.* **2003**, *50*, 55. (d) Qin, Y.; Pagba, C.; Piotrowiak, P.; Jäkle, F. *J. Am. Chem. Soc.* **2004**, *126*, 7015.

(13) Trecourt, F.; Mallet, M.; Mongin, F.; Queguiner, G. *Synthesis* **1995**, *9*, 1159.

(14) (a) Kumar, S.; Kim, T. Y. *J. Org. Chem.* **2000**, *65*, 3883. (b) Trecourt, F.; Mallet, M.; Mongin, F.; Queguiner, G. *Tetrahedron* **1995**, *51*, 11743. (c) Wallow, T. I.; Novak, B. M. *J. Am. Chem. Soc.* **1991**, *113*, 7411. (d) Goldschmid, H. R.; Musgrave, O. C. *J. Chem. Soc. C* **1970**, 488. (e) Liu, Q. D.; Jia, W. L.; Wu, G.; Wang, S. *Organometallics*, **2003**, *22*, 3781.

(15) (a) Suzuki, A. *Acc. Chem. Res*. **1982**, *15*, 178. (b) Miyaura, N.; Suzuki, A. *Chem. Rev.* **1995**, *95*, 2457.

(16) *SHELXTL NT Crystal Structure Analysis Package*, version 5.10; Bruker AXS, Analytical X-ray System: Madison, WI, 1999.

(17) (a) Cromer, D. T.; Waber, J. T. *International Tables for X-ray Crystallography*; Kynoch Press: Birmingham, AL, 1974; Vol. 4, Table 2.2A. (b) Spek, A. L. *Acta Crystallogr*., *Sect. A* **1990**, *46*, C34. (c) Spek, A. L. *Platon: A Multipurpose Crystallographic Tool*; Ultrecht University: Ultrecht, The Netherlands, 2005.

(18) Murov, S. L.; Carmichael, I.; Hug, G. L. *Handbook of Photochemistry*, 2nd ed.; Marcel Dekker: New York, 1993.

(19) Demas, N. J.; Crosby, G. A. *J. Am. Chem. Soc*. **1970**, *29*, 7262.

(20) (a) Pålsson, L.-O.; Monkman, A. P. *Adv. Mater*. **2002**, *14*, 757. (b) Mello, J. C.; Wittmann, H. F.; Friend, R. H. *Adv. Mater*. **1997**, *9*, 230.

(21) Pang, J.; Tao, Y.; Freiberg, S.; Yang, X.-P.; D'Iorio, M.; Wang, S. *J. Mater. Chem.* **2002**, 12, 206.

SCHEME 1

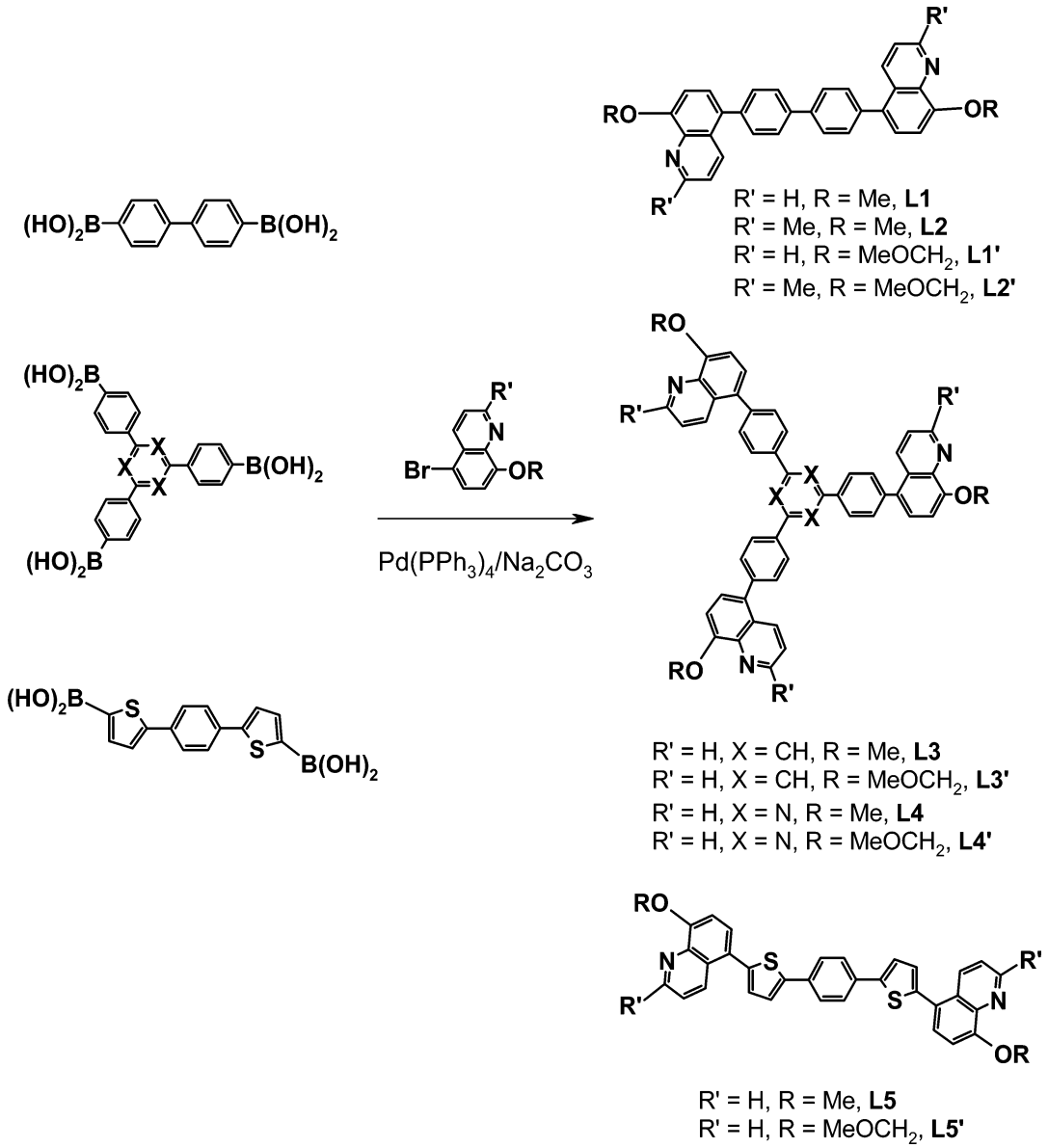

DMSO, which is most likely caused by intermolecular hydrogen bonding interactions of **L**(OH)**1**−**L**(OH)**5** in the solid state. Despite their poor solubility, ligands **L**(OH)**1**−**L**(OH)**5** were proven to be effective for chelation to a boron center. Previously we have demonstrated that the reaction of BPh_3 with 8-hydroxyquinoline and its derivatives (q′) can be used to synthesize the chelate boron compound BPh_2q and BPh_2q' readily.[11] Using similar procedures, BPh_3 was reacted with **L**(OH)**1**−**L**(OH)**5**, respectively, in refluxing THF, which resulted in the isolation of the corresponding chelate boron compounds **B1**−**B5**, respectively, in good yields, as shown in Scheme 2. The monoboron compound BPh_2(Ph-q) (**B0**) using the Ph-8-OH-q as the starting material was also prepared.

The ligands **L0**, **L1**−**L5** and the boron complexes **B0**, **B1**−**B5** were fully characterized by NMR (^{1}H and ^{13}C) and high-resolution MS spectroscopic analyses. To establish the hydrogen bonding patterns of **L**(OH)**1**−**L**(OH)**5** in the solid state, many attempts were made to grow their single crystals, but none were successful. Our attempts to obtain single crystals of the boron compounds **B1**−**B5** only resulted in the isolation of crystals that are too small for structural determination on our X-ray diffractometer. Nonetheless, single crystals of **L1**, **L3**, **L5**, and **B0** were obtained successfully, and their structures in the solid state were determined by single-crystal X-ray diffraction analyses.

Crystal Structures of L1, L3, L5, and B0. The molecular structures of **L1**, **L3**, and **L5** as determined by X-ray diffraction analyses are shown in Figures 1−5, respectively. The two linear molecules **L1** and **L5** possess a crystallographically imposed inversion center symmetry. The central cores (biphenyl, *p*-dithienylphenyl, respectively) in **L1** and **L5** are coplanar. The two 8-methoxyquinoline rings have an anti arrangement. The mean plane of the 8-methoxyquinoline ring in **L1** and **L5** is twisted ∼119.2° and ∼43.1°, respectively, relative to the central conjugated core. The relatively small dihedral angle in **L5** can be attributed to the diminished nonbonding interactions between the ortho hydrogen atoms of the central core and the hydrogen atoms of the quinoline ring, which, in turn leads to more efficient conjugation between the central core and the quinoline ring in **L5**, as reflected by the relatively short bond length (1.463(6)

SCHEME 2

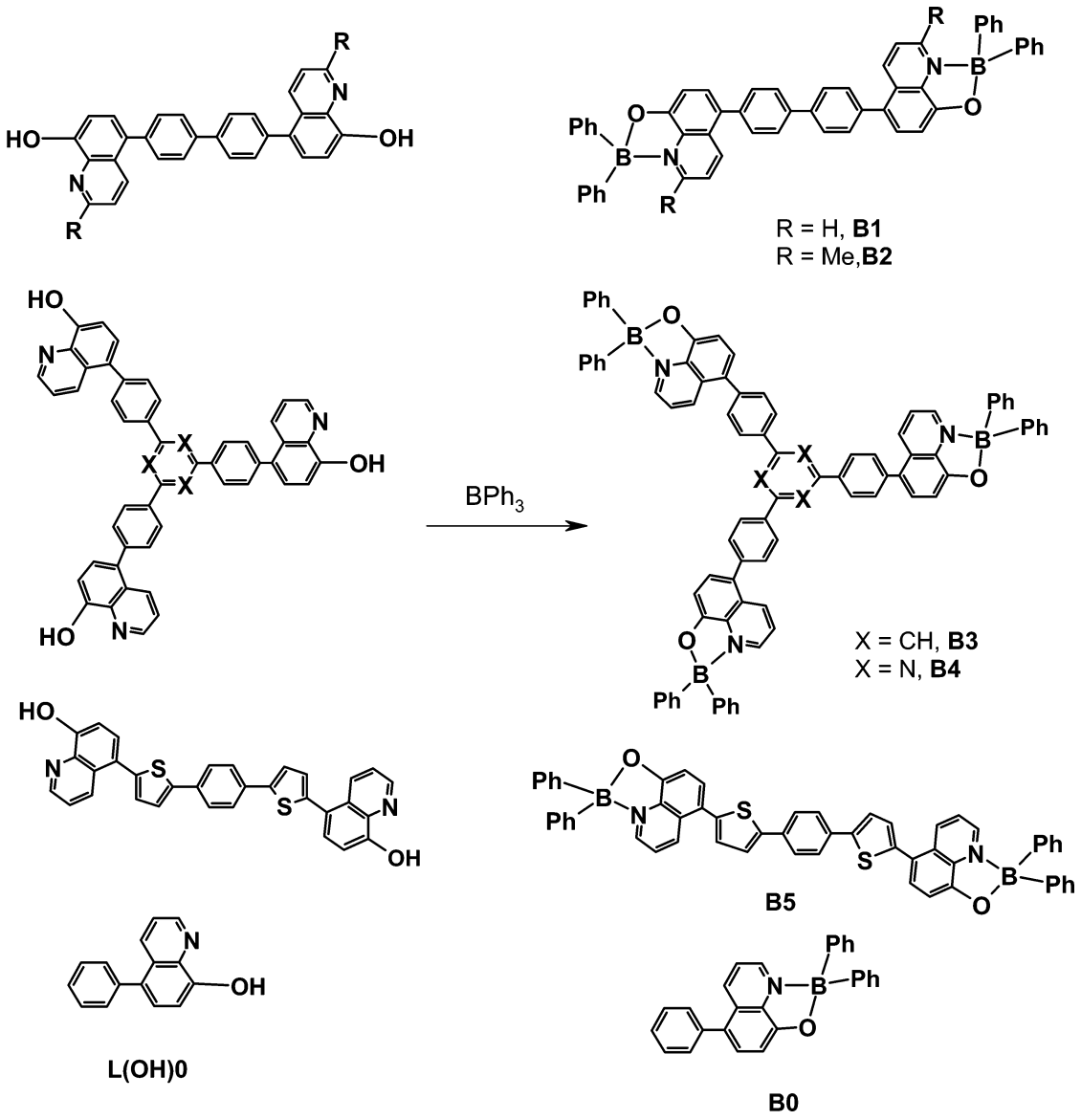

Å) of C(11)−C(5) in **L5** compared to that (1.496(3) Å) in **L1**. The triphenylbenzene central core in **L3** is not coplanar as indicated by the dihedral angles between the phenyl rings and the benzene core in **L3** of 39.5°, 68.6°, and 146.3°, respectively. The 8-methoxyquinoline moieties are also not coplanar with the adjacent phenyl rings (dihedral angles are 49.8°, 56.4°, and 60.5°, respectively).

L1, **L3**, and **L5** have distinct molecular packing patterns in the solid state. The linear molecules of **L1** all orient parallel to each other along the same direction with significant $\pi-\pi$ interactions between two adjacent 8-methoxyquinoline rings with the shortest atomic separation distance being 3.61(2) Å, as shown in Figure 1. The linear molecules of **L5** also orient parallel to each other in the crystal lattice. However, unlike the molecules of **L1** which have an extended linear architecture, the molecules of **L5** form a wavelike extended structure that propagates along the *c* axis as shown in Figure 5. A close examination reveals that the central cores of two adjacent molecules of **L5** are not parallel to each other but with a dihedral angle of 57.8°. However, the 8-methoxyquinoline rings between the two adjacent molecules in the crystal of **L5** have approximately parallel $\pi-\pi$ stacking interactions with the shortest separation distance being 3.50(2) Å. The star-shaped molecules of **L3** form interlocked pairs in the crystal lattice as shown in Figure 3, which further arrange into layered architecture. The most significant $\pi-\pi$ stacking interactions are again between the parallel 8-methoxyquinoline groups of interdigitated pairs with the shortest atomic separation distance being 3.71(2) Å.

The crystal structure of BPh_2(Ph-q) is shown in Figure 6. The tetrahedral coordination environment around the boron center is similar to the previously reported BPh_2q and BPh_2q′ compounds.[11] One important feature is that the 8-hydroxyquinolate ring has a dihedral angle of 55.2° and 61.4° with the phenyl ring, for the two independent molecules in the asymmetric unit, respectively, which are similar to those observed in **L1**.

Physical, Electronic and Photophysical Properties. Our investigation on physical, electronic, and photophysical properties of the new compounds focused on the 8-methoxyquinoline series **L1**−**L5** and their corresponding boron compounds. The properties of **L1′**−**L5′** closely resemble those of **L1**−**L5**, thus they are not presented here. For the 8-hydroxyquinoline series **L**(OH)**1**−**L**(OH)**5**, it is difficult to investigate their properties

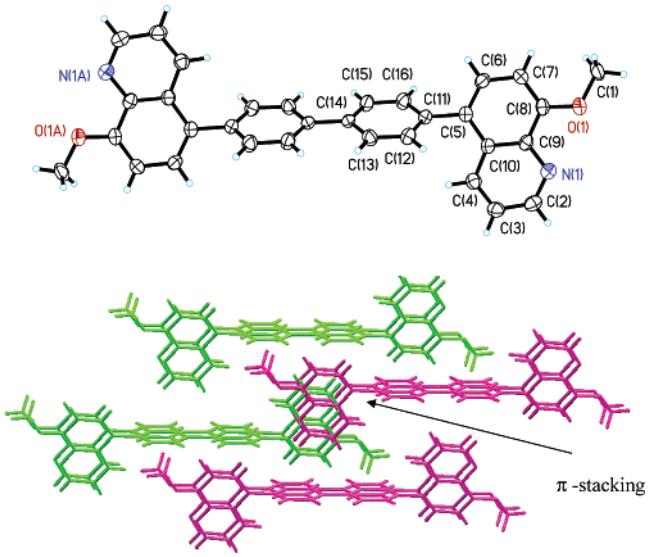

FIGURE 1. A diagram showing the molecular structure of **L1** with labeling schemes (top) and the packing diagram showing intermolecular $\pi-\pi$ interactions (bottom).

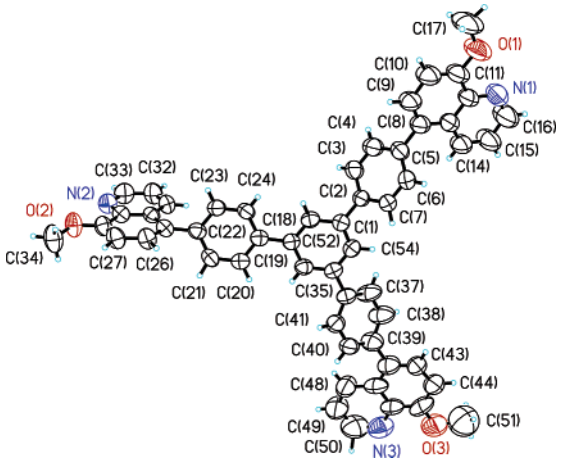

FIGURE 2. A diagram showing the molecular structure of **L3** with labeling schemes.

because of their insolubility in common organic solvents. The data of the ligands **L1**−**L5** provide a good comparison to those of the boron compounds, thus allowing us to appreciate the impact of the chelation by the BPh_2 group. One noteworthy feature for **L1**−**L5** and **B1**−**B5** is that albeit being small molecules, they can form transparent films readily on a glass substrate by a simple spin coating process. Between the two groups of compounds, the boron compounds form better and more uniform films than the free ligands. To compare the difference between the diboron compound **B1** and the monoboron compound **B0**, the properties of **B0** and corresponding free ligand **L0** were also investigated.

Thermal Properties. The thermal stability of ligands **L1**−**L5** and the corresponding boron compounds **B1**−**B5** were examined by DSC and TGA. No melting points and glass transition temperatures up to 300 °C were observed for **L1**−**L5** in the DSC diagrams. TGA experiments confirmed that ∼3% weight loss occurs at the temperature range of 302−380 °C for all the ligands, an indication that **L1**−**L5** are thermally stable up to ∼300 °C. Similar to **L1**, the molecule **L0** does not display

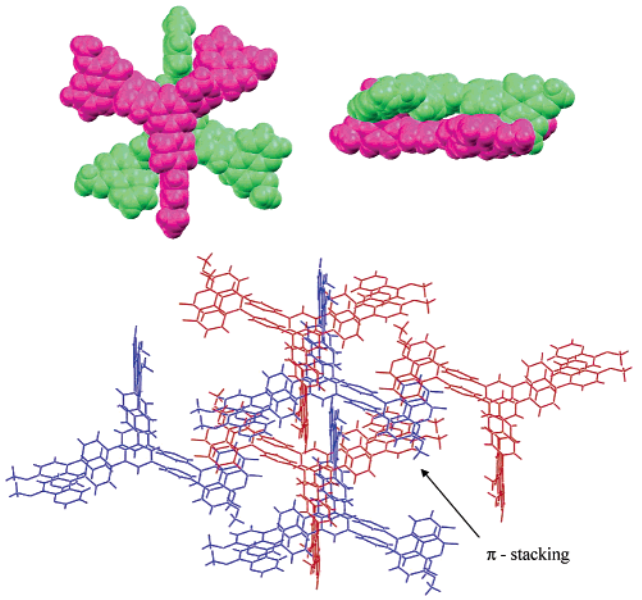

FIGURE 3. Diagrams showing the interlocked pair of **L3** (left, top view; right, side view) (top) and the packing diagram showing intermolecular $\pi-\pi$ interactions (bottom).

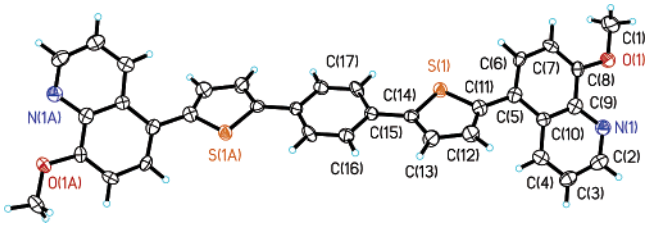

FIGURE 4. A diagram showing the molecular structure of **L5** with labeling schemes.

any melting point. However, it undergoes complete sublimation at ∼163°C and one atmosphere, which is clearly due to its much smaller molecular weight, compared to **L1**. The boron complexes **B1**−**B5** exhibited similar thermal properties as the free ligands with the thermal decomposition temperature in the range of 307−346 °C. The monoboron compound **B0** has a decomposition temperature of 261 °C, significantly lower than the diboron compound **B1**. This enhanced thermal/morphological stability for the diboron compound can be attributed to the increased molecular weight and the extended intermolecular interactions of the linear molecule **B1**. TGA diagrams for all compounds are provided in supporting materials.

Absorption Spectra. Ligands. All free ligands display intense absorption bands in the UV region with the absorption maxima at ∼280 to 300 and 330−340 nm as shown in Figure 7, which can be attributed to $\pi-\pi^*$ electronic transitions. Ligands **L1**−**L4** have no significant absorption at $\lambda > 400$ nm while one of the absorption bands of **L5** covers the 300−450 nm region, which is consistent with the fact that **L1**−**L4** are colorless while **L5** is yellow. Using the absorption edge, the optical energy gaps for **L1**−**L5** were estimated to be 3.26, 3.29, 3.30, 3.08, and 2.80 eV, respectively. The star-shaped molecule with a triazine core **L4** has a smaller band gap than the benzene core analogue **L3**, which is consistent with the general trend observed previously for star-shaped molecules with triazine and benzene cores.[21] The small band gap of **L5** is due to the involvement of the thienyl groups and the greater degree of

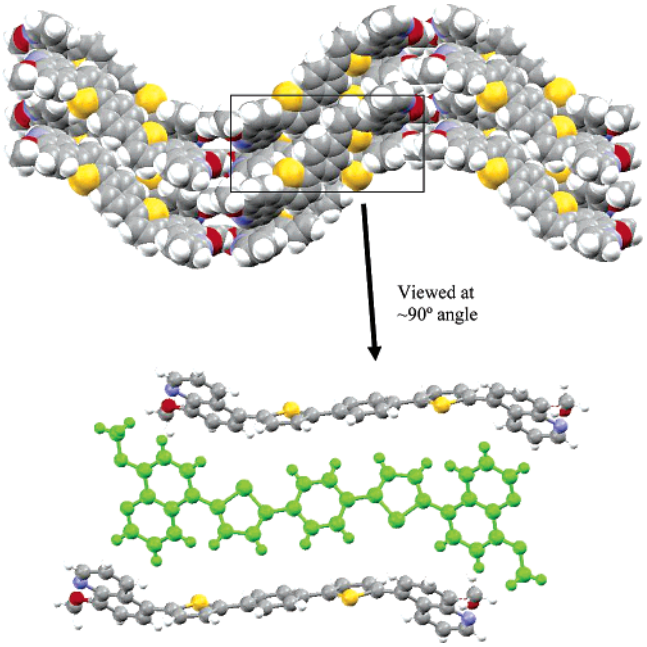

FIGURE 5. A space-filling packing diagram showing the intermolecular $\pi-\pi$ interactions and the wavelike arrangement of molecule **L5** in the crystal lattice (top); detail of the enlarged area viewed at ~90° angle (bottom).

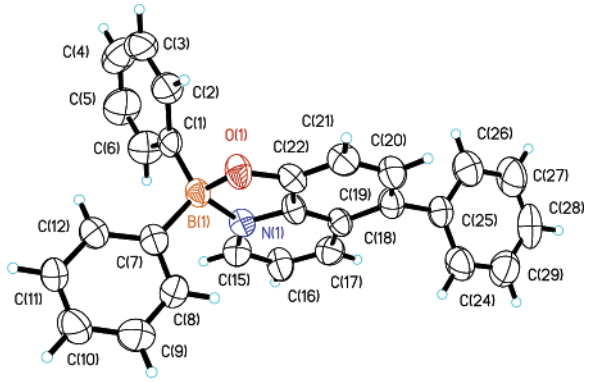

FIGURE 6. A diagram showing the molecular structure of BPh_2(Phq) with labeling schemes.

conjugation in **L5**, compared to other ligands. The **L0** molecule has a band gap of 3.37 eV which is significantly bigger than that of **L1**.

Boron Compounds. In contrast to the free ligands, the boron compounds are all colored: **B1**−**B4** are yellow-green in solution while **B5** is yellow-orange, consistent with the presence of an absorption band in the 340−550 nm region. The color change from the free ligand to the boron compound is due to the decrease of the HOMO−LUMO energy gap, as confirmed by the band gap energy obtained from the absorption edge for **B1**−**B5** (2.58, 2.64, 2.48, 2.57, and 2.38 eV, respectively) which is about 0.50−0.70 eV smaller than the corresponding free ligand. The band gap of **B1** is comparable to the related monoboron compound **B0** (2.54 eV). The somewhat bigger band gap of **B2**, compared to that of **B1**, is consistent with the previous observation that the 2-methyl group on the hydroxyquinolate ligand leads to a small blue shift of the band gap.[11a] The decrease of the HOMO−LUMO gap in the boron compounds is due to the fact that the ligands in the complexes are anionic, which is

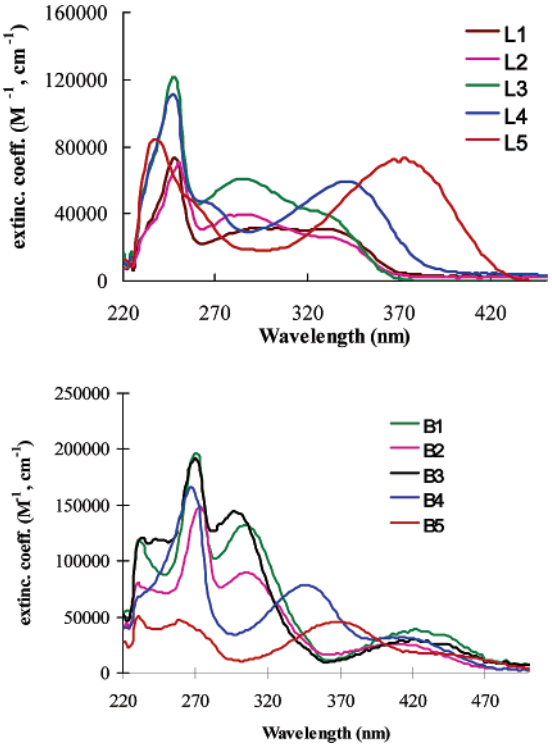

FIGURE 7. The UV−vis spectra of **L1**−**L5** in CH_2Cl_2 (top) and the UV−vis spectra of **B1**−**B5** in CH_2Cl_2 (bottom).

known to have a smaller band gap compared to the neutral ligand, on the basis of similar observation of BPh_2q and BPh_2q'.[11] The role of the boron center is simply to stabilize the anionic ligand. Consistent with the trend of the free ligands, the boron compound **B5** has the smallest band gap, and its absorption band tails to 540 nm. The absorption data and optical band gaps for **L1**−**L5** and **B1**−**B5** are provided in Table 1 and Table 2.

Electrochemical Properties. Ligands. To estimate the HOMO and LUMO energy levels and to examine the stability of the reduced and oxidized species of the free ligands and the boron compounds in solution, cyclic voltammetric diagrams were recorded. Ligands **L1**−**L2** display two similar and well resolved irreversible oxidation peaks with the first one at 1.46 V and the second one at 1.80 and 1.83 V, respectively, which may be attributable to the sequential oxidation of the two quinolate rings. To determine if the two oxidation peaks displayed by **L1** are indeed due to the oxidation of the quinolate groups, the CV diagram of the **L0** molecule was recorded, which displays a single oxidation peak at 1.70 V within the solvent limit window (−2.0 to +2.0 V) which is at about midpoint of the two oxidation peaks displayed by **L1**. This led us to believe that the relatively low first oxidation potential and the presence of two oxidation peaks in **L1** are a consequence of electronic communication between the two quinolate groups mediated via the biphenyl link. Hence, increasing the number of chromophores linked via aromatic groups clearly has a significant impact on the HOMO level of the molecule. The first oxidation potential (1.45 V) of the star-shaped **L3** is nearly identical to those of **L1** and **L2**. However, its second oxidation potential (1.88 V) is slightly higher than those of **L1** and **L2**, which can be attributed to the low degree of conjugation of the central triphenylbenzene core in **L3** as revealed by the crystal structure, compared to the coplanar biphenyl core in **L1** and **L2**. (Although

TABLE 1. UV−Visible and Emission Data for L1−L5 and B1−B5

compds	UV−vis[a] (λ_{max}, nm)	emission (λ_{max}, nm)	quantum yield/(Φ_{em}, %) CH_2Cl_2[b]	quantum yield/(Φ_{em}, %) SSQE[c]	conditions
L0/B0	246, 322/230, 268, 414	405/530	89/13	N/A	CH_2Cl_2, 298 K
		388/525	N/A	N/A	film, 298 K
L1/B1	294,330/230, 270, 304, 418	415/537	68/10		CH_2Cl_2, 298 K
		418/536		23/6	film, 298 K
L2/B2	308,332/258, 306, 406	409/529	79/23		CH_2Cl_2, 298 K
		416/513		20/8	film, 298 K
L3/B3	282,330/242, 270, 298, 416	413/533	61/15		CH_2Cl_2, 298 K
		422/531		21/6	film, 298 K
L4/B4	340/266, 346, 420	445/528	63/23		CH_2Cl_2, 298 K
		456/508		10/11	film, 298 K
L5/B5	340/234, 260, 366, 430(s)	462/594	20/1		CH_2Cl_2, 298 K
		486/593		8/3	film, 298 K

[a] Concentration: [M] = 5×10^{-6} M. [b] Using anthracene as the standard for **L0** and 9,10-diphenylanthracene as the standard for the remaining compounds in CH_2Cl_2 at room temperature. [c] Solid State Quantum Efficiency (SSQE) were measured from ligands films spin cast onto fused silica substrates from chloroform solutions.

TABLE 2. Electrochemical Data and Experimental and Theoretical (MO) HOMO/LUMO Energy Level

	L1	L2	L3	L4	L5
E_{ox} (V)[a]	1.46, 1.80	1.46, 1.83	1.45, 1.88	1.51	1.27, 1.95
E_{red} (V)[a]	N/A	N/A	N/A	−1.73	−1.33
electrochemical ΔE (eV)	N/A	N/A	N/A	3.24	2.60
optical ΔE (eV)[b]	3.26	3.29	3.30	3.08	2.80
MO ΔE (eV)	4.06	4.07	4.14	3.65	3.46
LUMO (eV) exptl[c]/MO	−2.50/−1.58	−2.50/−1.49	−2.45/−1.58	−2.73/−2.17	−2.83/−1.89
HOMO (eV) exptl[d]/MO	−5.76/−5.64	−5.79/−5.56	−5.75/−5.72	−5.81/−5.82	−5.63/−5.35

	B1	B2	B3	B4	B5
E_{ox} (V)[a]	1.45	1.45	1.53	1.49	1.10
E_{red} (V)[a]	−1.62	−1.80	−1.46	−1.58	−1.25, −1.60
electrochemical ΔE (eV)	3.07	3.25	2.99	3.07	2.35
optical ΔE (eV)[b]	2.55	2.64	2.48	2.57	2.38
LUMO (eV) exptl[c]	−3.20	−3.11	−3.28	−3.21	−3.02
HOMO (eV) exptl[d]	−5.75	−5.75	−5.76	−5.78	−5.40

[a] Measured in CH_2Cl_2, except **B3** which was measured in DMF: $Bu_4N[PF_6]$ as the electrolyte; AgCl/Ag as the reference electrode. [b] Recorded in CH_2Cl_2 with a concentration $\approx 10^{-6}$ M. [c] From the optical band gap and the HOMO energy. [d] From the oxidation potential, calibrated using the oxidation potential and the absolute HOMO energy level of $FeCp_2$.

the oxidation may be localized on the quinoline portion, because of its partial conjugation with the phenyl or biphenyl group of the central core, the oxidation potential can be affected by the degree of conjugation through the entire molecule.) For **L4** the first oxidation potential (1.51 V) is significantly higher than those of **L1**−**L3** and the second oxidation potential of **L3**, > 2.0 V, is beyond the solvent limit for measurement, which is caused by the electronegative central triazine ring that stabilizes the HOMO level, compared to the biphenyl or the benzene core in **L1**−**L3**. For **L5**, the first oxidation potential (1.27 V) is much lower than those of **L1**−**L4** and can be attributed to the oxidation of the thienyl-containing central ring. The oxidation peak of the 8-methoxyquinoline ring in **L5** is not resolved. For compounds **L1**−**L3**, no reduction peaks within the solvent limit (−2.0 V) were observed. For **L4** a quasi-reversible reduction peak was observed at −1.73 V, which can be attributed to the reduction of the central triazine core. Clearly the electronegative triazine ring lowers the LUMO level significantly, compared to the benzene core analogue **L3**. For **L5**, an irreversible reduction peak was observed at −1.33 V, which may be due to the reduction of the central core. Selected CV diagrams for **L1**−**L5** are shown in Figure 8. The electrochemical data along with the absolute energy (eV) converted by using the ferrocene redox couple as the standard are shown in Table 2. On the basis of the electrochemical data, ligands **L4** and **L5** may be suitable as

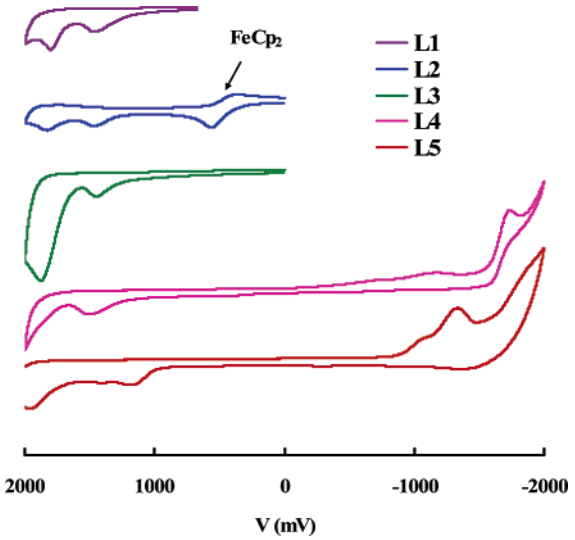

FIGURE 8. The CV diagrams for **L1**−**L5** recorded in CH_2Cl_2.

electron transport materials because of their relatively deep LUMO levels.

Boron Compounds. The CV diagrams for all boron compounds (Figure 9) were recorded in CH_2Cl_2 except **B3** whose

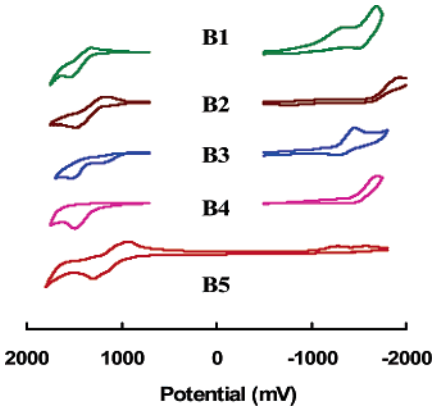

FIGURE 9. The CV diagrams for **B1**, **B2**, **B4**, and **B5** recorded in CH_2Cl_2 and for **B3** in DMF.

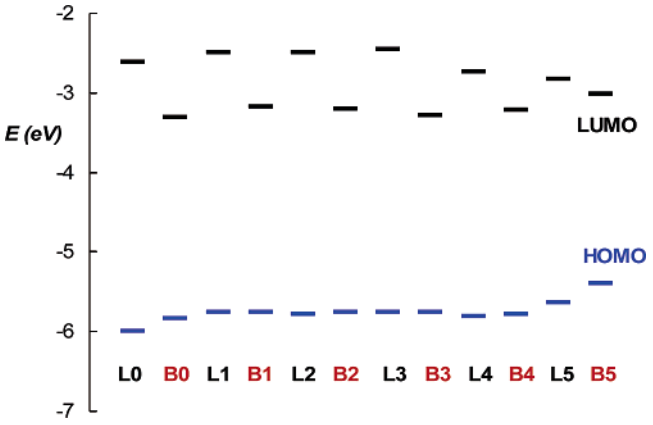

FIGURE 10. The experimental HOMO and LUMO levels for **L1**−**L5** and **B1**−**B5**.

CV diagram was recorded in DMF because of its poor solubility in CH_2Cl_2. Reversible or quasi-reversible oxidation peaks were observed for the boron compounds **B1**−**B3** and **B5**. The fact that most of the boron compounds display a reversible oxidation peak indicates that the oxidized species of the boron compounds are more stable than those of the free ligands. The oxidation potentials for all boron compounds were converted to HOMO energies using ferrocene as the standard. As shown in Table 2, the HOMO energies of the boron compounds are similar to those of the corresponding free ligands except **B5** which has a considerably higher HOMO level than that of **L5**. Quasi-reversible reduction peaks for most boron compounds were observed. The reduction potentials of the boron compounds are in general much less negative than those of the corresponding free ligands. In fact the distinct difference between the free ligands and the boron compounds is the LUMO energy level.

For all boron compounds, the LUMO level is about 0.20 to 0.70 eV lower than that of the corresponding ligand, which indicates that the chelation by the Lewis acid boron center to the ligands **L1**−**L5** significantly stabilizes the LUMO level and makes the boron compounds potentially better electron transport materials than the free ligands. Previously we have demonstrated that monoboron BPh_2q and BPh_2q' compounds could function effectively as electron transport materials in OLEDs while the corresponding free ligands were not effective as electron transport materials in OLEDs.[11] The role of the boron center in these compounds is parallel to the role of the Al(III) center in the well-known electron transport compound Alq_3—stabilizing the anionic ligand q and lowering the LUMO level. The reversibility of the redox waves of the boron complexes indicates that they are electrochemically more stable than the free ligands toward reduction, which can be again attributed to the presence of the Lewis acid boron center in the complexes. The monoboron compound **B0** displays an oxidation and a reduction peak in CH_2Cl_2 at 1.64 and −1.67 V, respectively. The key difference between this molecule and the related diboron molecule **B1** is the significant decrease of the oxidation potential in the diboron compound (corresponding to about 0.2 eV increase of the HOMO level), which can be again contributed to the presence of electronic communication between the two boron chelate chromophores in the diboron compound.

As shown by the experimental HOMO and LUMO energy level diagram in Figure 10, for the free ligands, there is little variation on the HOMO level but substantial decrease on the LUMO level for **L4** and **L5**. The coordination by the boron center causes some degree of destabilization of the HOMO level but dramatic stabilization of the LUMO level, and the net decrease of the band gap, compared to those of the free ligands.

Molecular Orbital Calculations for L1−**L5.** To gain a deeper understanding on the electronic properties of molecules **L1**−**L5**, molecular orbital calculations of ligands have been performed using Gaussian 98 (DFT), B3LYP parameters, and the 6-311G** basis set.[22] The initial geometric parameters for **L1**, **L3**, and **L5** used in the calculations were from crystal data and were allowed for further geometry optimization. The geometric parameters for **L2** were calculated by using the coordinates of **L1** and replacing the hydrogen atoms at C-2 positions of the methoxyquinoline moieties with two CH_3 groups. Similarly, geometric parameters of **L4** were obtained by replacing the three C−H in the central benzene ring of **L3** with three N atoms. The final geometric parameters for **L2** and **L4** were obtained by geometry optimization. As shown by the data in Table 2, the general trend of the HOMO/LUMO energies obtained from the calculations is in agreement with that obtained from experimental data, although there are considerable deviations between the calculated values and the observed data. The diagrams of HOMO and LUMO orbitals of **L1**, **L3**, **L4**, and **L5** are shown in Figure 11. For the linear ligands **L1** (**L2** is very similar to that of **L1**) and **L5**, the HOMO and the LUMO levels involve contributions from the entire molecule. The lowest electronic transition in these molecules can be therefore considered as $\pi-\pi^*$ transitions. For the star-shaped molecule of **L3** with a central benzene core, the HOMO and LUMO levels can also be considered as π and π^* orbitals, respectively, involving the entire molecule. In contrast, however, the HOMO and the LUMO levels of **L4** with a triazinie core are quite different: the HOMO involves contributions from the three 8-methoxyquinoline legs, but little contributions from the central triphenyltriazine core while the LUMO is dominated by the triphenyltriazine core with little contributions from the three 8-methoxyquinoline legs. On the basis of this, the lowest electronic transition in **L4** is most likely charge-transfer between the peripheral 8-methoxyquinoline legs and the central electronegative triazine ring. Although molecular orbital calculations for the boron compounds **B1**−**B5** were not performed because of their large sizes, the frontier orbitals of the boron compounds

(22) (a) Beck, A. D. *J. Chem. Phys.* **1993**, *98*, 5648. (b) Lee, C.; Yang, W.; Parr, R. G. *Phys. Rev. B: Condens. Matter Mater. Phys.* **1988**, *37*, 785.

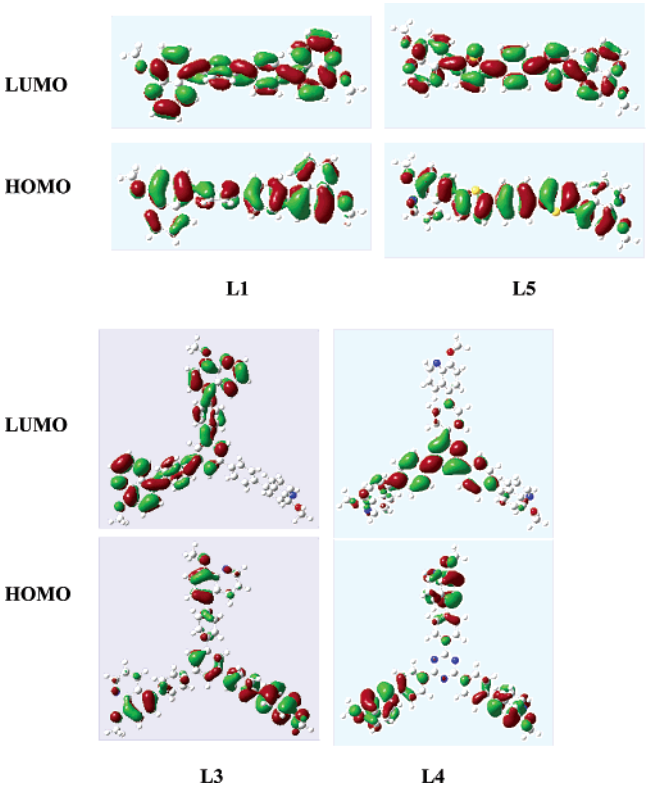

FIGURE 11. HOMO and LUMO diagrams for **L1**, **L3**, **L4**, and **L5.**

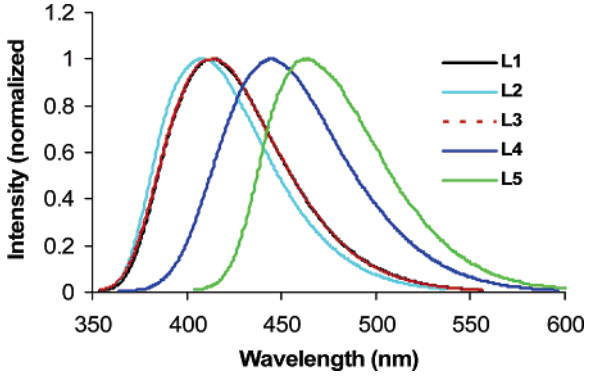

FIGURE 12. Emission spectra of **L1**−**L5** recorded in CH_2Cl_2 (∼10^{-6} M).

TABLE 3. Solvent Effects on Emission of L1−L5 and B1−B5 (∼10^{-6} M)

solvents	L1/B1	L2/B2	L3/B3	L4/B4	L5/B5
toluene	406/532	403/524	406/527	419/519	456/587
CH_2Cl_2	416/537	408/524	413/533	443/522	462/594
DMF	421/539	413/532	419/538	483/524	471/600

should resemble those of the corresponding ligands, on the basis of our earlier investigation on mononuclear BPh_2q and BPh_2q' compounds.[11a]

Luminescent Properties. Ligands. When irradiated by UV light, the free ligands **L1**−**L5** emit a blue light in solution and in the solid state. The fluorescent spectra of the ligands are shown in Figure 12. In solution, the emission energy of **L1**−**L3** shows a relatively small red shift with the increase of the solvent polarity, as shown by data in Table 3. In contrast, a dramatic red shift by **L4** and **L5** with the solvent polarity was

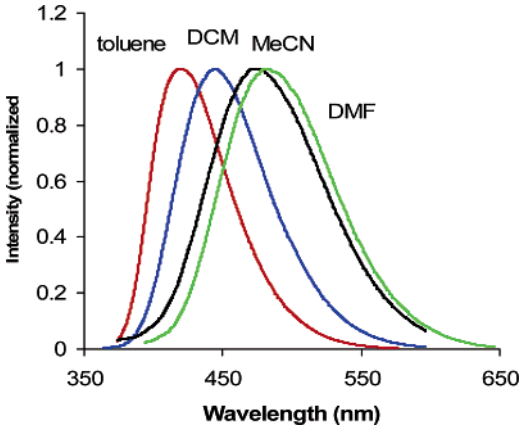

FIGURE 13. Solvent dependent emission spectra of **L4** (∼10^{-6} M).

observed (Figure 13). For **L4**, this is understandable since the lowest electronic transition is charge transfer between the 8-methoxyquinoline leg and the central triazine core. For **L5** it is not yet understood what the origin of the large red shift of emission energy is. One possibility is the change of molecular conformation of **L5**. In the solid state, as shown by the crystal structure, the two thienyl groups in **L5** have an anti arrangement. Molecular orbital calculations also confirmed that this is indeed the preferred conformation. In solution, the molecule likely undergoes rapid interconversion of different molecular conformations and some of the nonplanar conformations may indeed lead to charge-transfer emission that is solvent polarity dependent. In CH_2Cl_2, **L1**−**L4** are efficient blue emitters with λ_{max} = 409−445 nm and the quantum yield being 61−79%. In contrast, the thienyl-containing molecule **L5** has a relatively low quantum yield (20%) and the longest emission wavelength (λ_{em} = 462 nm) among the five free ligands, which can be attributed to the presence of the heavy sulfur atoms in **L5** that can reduce the fluorescent quantum efficiency via "heavy atom effects". The high rotational flexibility between the two thienyl groups may also be responsible for the low emission quantum efficiency of **L5**. A similar phenomenon has been observed in the mononuclear BPh_2q' compounds where thienyl functionalized hydroxyquinoline compounds have a low quantum efficiency.[11a] The molecule **L0** emits at 405 nm in CH_2Cl_2, which is about 10 nm blue-shifted, compared to **L1**, attributable to the increased conjugation and the presence of two quinolate chromophores in **L1**.

The emission spectra of **L1**−**L5** in the solid-state resemble those of solutions, but are red-shifted by 10−20 nm. **L5** experiences the largest red shift among all the ligands, which can be attributed to intermolecular interactions as demonstrated by the crystal structures of **L1**, **L3**, and **L5**. Further evidences for the presence of intermolecular interactions are the significant lower quantum yields of the ligands in the solid state (8−23%), compared to those measured in CH_2Cl_2. Again, the thienyl-containing ligand **L5** has the lowest quantum yield in the solid state. Intermolecular $\pi-\pi$ interactions that significantly red-shift emission energy and lower the emission quantum yield have been frequently observed previously.[23] Although molecules **L1**−**L4** are bright blue emitters in solution and have a high

(23) (a) Brinkmann, M.; Gadret, G.; Muccini, M.; Taliani, C.; Masciocchi, N.; Sironi, A. *J. Am. Chem. Soc*. **2000**, *122*, 5147. (b) Wang, R. Y.; Jia, W. L.; Aziz, H.; Vamvounis, G.; Wang, S.; Hu, N. X.; Popović, Z. D.; Coggan, J. A. *Adv. Funct. Mater.* **2005**, *15*, 1483.

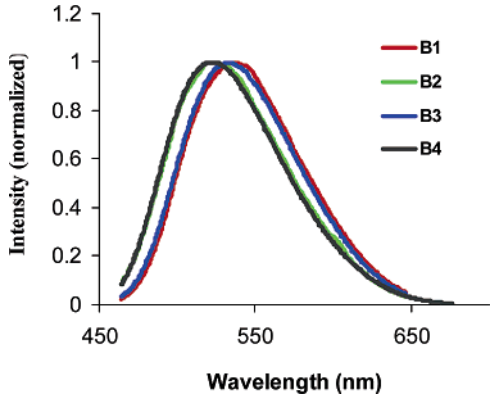

FIGURE 14. Emission spectra of **B1**−**B4** recorded in CH_2Cl_2 (~10^{-6} M).

thermal stability, the strong intermolecular interactions in the solid-state hamper their use as blue emitters in OLEDs because of the low quantum efficiency in the solid state. On the other hand, strong intermolecular interactions can facilitate charge transport in OLEDs, if the molecules can undergo reversible oxidation (hole transport) or reduction (electron transport). For **L4**, the reduction peak is quasi-reversible, which along with the relatively low LUMO level makes it a potential candidate for electron transport. The fluorescent spectra of the free ligands do not show significant change with concentration or temperature.

Boron Compounds. In contrast to the free ligands which emit in the blue region, the boron compounds **B1**−**B4** emit in the green region (λ_{em} = 528−542 nm) in CH_2Cl_2 which do not change significantly with concentration (Figure 14). For compound **B5**, however, the emission color is dependent on the concentration of the solution. Compared to the free ligands, especially **L4** and **L5**, the red-shift of the emission spectra of the boron compounds with the increase of the solvent polarity is much less pronounced as shown by Table 3, an indication of a decreased polarity of the excited state in the boron compounds. For **B4**, this can be explained by the coordination of the boron center to the hydroxyquinoline chelate site which effectively reduces the electron density on the hydroxyquinoline leg, thus reducing the polarity of the charge transfer in excited state, compared to that of **L4**. In the solid state, the emission spectra of **B1**−**B4** either experience no change or a small blue shift, compared to the solution emission spectra. For compound **B5**, however, a dramatic red shift was observed which will be further discussed below. Among the five boron complexes, **B4** has the highest luminescent efficiency both in solution (23% in CH_2Cl_2) and in the solid state (11%), while **B5** has the lowest luminescent efficiency (1% in CH_2Cl_2 and 3% in solid state) at room temperature. The boron compounds are in general less efficient as emitters in solution than the corresponding ligands as shown by data in Table 1.

Concentration-Dependent Emission of B5. The most interesting observation for the boron compounds is the concentration dependent emission of **B5**. As shown by Figure 15 (top), in the low concentration range (1.0×10^{-7} to 5.0×10^{-6} M), the emission maximum of **B5** is at ~462 nm, and the emission intensity increases linearly with the increase of concentration. Interestingly, however, as the concentration is increased to above 5.0×10^{-6} M, the emission energy shifts gradually to a longer wavelength, accompanied by a substantial decrease of the emission intensity (Figure 15, bottom). At the concentration of

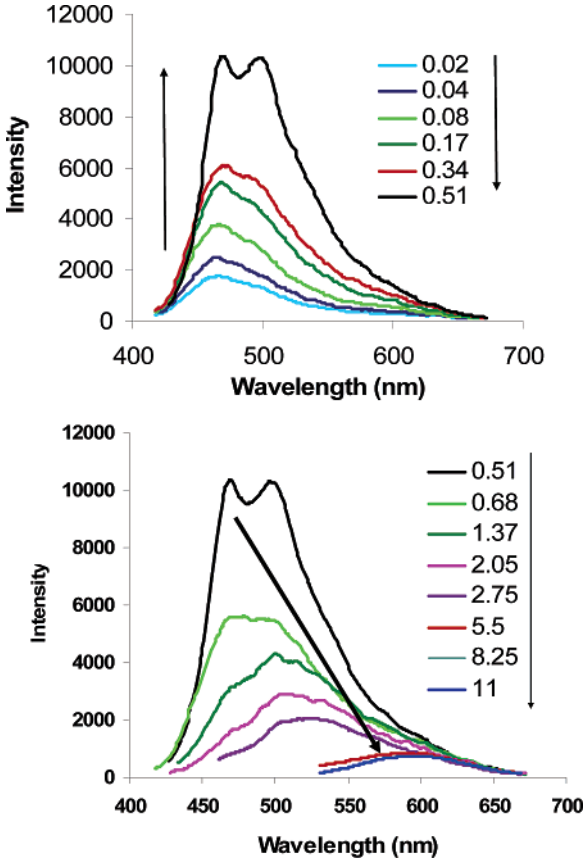

FIGURE 15. Emission spectral change of **B5** with concentration in CH_2Cl_2: (top) the low concentration range (0.02×10^{-5} to 0.51×10^{-5} M); (bottom) the high concentration range (0.51×10^{-5} to 11×10^{-5} M).

5.0×10^{-5} M, the emission maximum of **B5** is at 593 nm, about a 130 nm red-shift from the low concentration emission peak. The high concentration emission spectrum of **B5** is in fact identical to its emission spectrum in the solid state. The phenomenon of the concentration dependent emission can be therefore attributed to intermolecular interactions of **B5** which become significant at high concentrations. Although the crystal structure of **B5** was not determined owing to the lack of suitable single crystals, intermolecular $\pi-\pi$ interactions as revealed by the crystal structure of **L5** must be responsible for the concentration dependence of the emission spectrum of **B5**. It is not understood yet why the free ligand **L5** does not display similar concentration-dependent emission. It is noteworthy that the absorption spectra of **B5** are essentially identical from the solution to the solid state (the same is also true for **B1**−**B4** and the free ligands), indicative of that intermolecular interactions have a dramatic impact on the excited state of the boron compound **B5**, but not on the ground state (see Supporting Information). The concentration induced red shift of **B5** is therefore likely caused by the formation of excimers in the high concentration range.[24]

Temperature-Dependent Emission of the Boron Compounds. Most of the boron compounds except **B5** experience a

(24) (a) Sims, M.; Bradley, D. D. C.; Ariu, M.; Koeberg, M.; Asimakis, A.; Grell M.; Lidzey, D. G. *Adv. Funct. Mater.* **2004**, *14*, 765. (b) Jaramillo-Isaza, F.; Turner, M. L. *J. Mater. Chem.* **2006**, *16*, 83. (c) Lakowicz, J. R. *Principles of Fluorescence Spectroscopy*, 2nd ed.; Kluwer Academic/Plenum: New York, 1999.

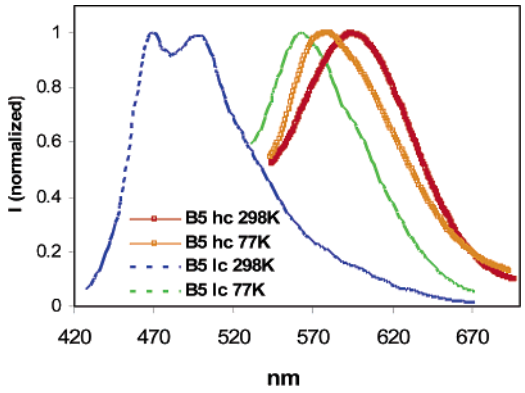

FIGURE 16. Temperature-dependent emission for **B5** at low concentration (lc) (5.0×10^{-6} M) and at high concentration (hc) (5.0×10^{-5} M) in CH_2Cl_2.

blue shift of the emission energy from ambient temperature to low temperature in solution. For example, the linear molecule **B1** emits at 537 nm at ambient temperature which is shifted to 515 nm at 77 K. The blue shift of emission energy at low temperature can be generally attributed to the increased environmental rigidity and has been observed in other systems previously.[25] Similarly, in the solid state, the emission energy of all boron compounds experience a blue shift when the temperature is lowered to 77 K.

The temperature-dependent emission of **B5** is influenced by concentration. In the low concentration range (1.0×10^{-7} to 5.0×10^{-6} M), the emission maximum of **B5** shifts from blue (462 nm) at ambient temperature to yellow (564 nm) at 77 K. In the high concentration range ($>5.0 \times 10^{-5}$ M), the emission color changes from red-orange (595 nm) at ambient temperature to orange (579 nm), as shown in Figure 16. The red shift of the low concentration sample with the decrease of temperature is clearly associated with the increased intermolecular interactions at low temperature. The blue shift of the high concentration sample can be explained as following. As shown by Figure 14, the intermolecular interactions of **B5** reach saturation at concentrations greater than 5.0×10^{-5} M at ambient temperature, thus, further decreasing the temperature does not cause any further red shift of the emission energy. On the other hand, the decrease of the temperature increases the environmental rigidity, thus causing a blue shift of the emission energy, as observed for other boron compounds.

The dramatic color change of **B5** from blue to red-orange with concentration and temperature is rare in main group organometallic compounds, although similar phenomena have been frequently observed in extended transition metal chain compounds where the emission color changes with the degree of metal−metal interactions that are dictated by concentration and temperature.[25a,26] This unique temperature-dependent property of **B5** makes it a potential candidate as a fluorescent temperature sensor.

(25) (a) Wang, S.; Garzon, G.; King, C.; Wang, J. C.; Fackler, J. P., Jr. *Inorg. Chem.* **1989**, *28*, 4623. (b) Lees, A. J. *Chem. Rev.* **1987**, *87*, 711 (c) Ferraudi, G. J. *Elements of Inorganic Photochemistry*; John Wiley & Sons: New York, 1988. (d) Liu, Q.-D.; Madadu, M. S.; Thummel, R.; Tao, Y.; Wang, S. *Adv. Funct. Mater.* **2005**, *15*, 143.

(26) (a) Assefa, Z.; Omary, M. A.; McBurnett, B. G.; Mojamed, A. A.; Patterson, H. H.; Staples, R. J.; Fackler, J. P., Jr. *Inorg. Chem.* **2002**, *41*, 6274. (b) Omary, M. A.; Patterson, H. *Inorg. Chem.* **1998**, *37*, 1060.

Conclusions

We have demonstrated that by incorporating more than one 8-hydroxyquinolate groups into a linear or star-shaped central core, the thermal stability of the molecule can be greatly enhanced. The linear and star-shaped molecules of **L1**−**L5** have highly anisotropic layered structures in the crystal lattice as confirmed by the crystal structures **L1**, **L3**, and **L5** (The structures of **L2** and **L4** are very likely to be similar to their analogues **L1** and **L3**, respectively.). The extended intermolecular interactions as established by the crystal structures are believed to be responsible for the enhanced thermal/morphological stability and the significantly diminished luminescent efficiency of these new organic molecules in the solid state. Compounds **L4** and **L5** have a fairly low LUMO level, which along with their strong intermolecular interactions makes them potential electron transport materials. The chelation by boron centers to molecules **L1**−**L5** does not have a great impact on thermal properties but dramatically decreases the LUMO levels, thus making the boron compounds **B1**−**B5** better candidates as electron transport materials. Furthermore, the chelation by the boron center substantially decreases the HOMO−LUMO band gap and red-shifts the emission energy, compared to the free ligands. The key difference between the polyboron compounds and the monoboron **B0** reported here and the monoboron compounds reported previously is the enhanced thermal stability and the dramatic temperature and concentration dependent phenomena as amplified by **B5**, which is clearly caused by the much enhanced intermolecular interactions in the polyboron compounds. Furthermore, the inclusion of polychromophores or polyboron centers that are linked together by an aromatic group appears to have significant impact on the HOMO level of the molecule, as demonstrated by **L0** and **L1** and **B0** and **B1**.

Experimental Section

All solvents were freshly distilled over appropriate drying agents prior to use. Reactions that required oxygen-free conditions were carried out under nitrogen using standard Schlenk techniques. ^1H and ^{13}C NMR spectra were recorded on either a 300 MHz or a 400 NMR spectrometer. High-resolution mass spectra were recorded on a mass spectrometer equipped with an electrospray source. **L1**−**L5** MS data were recorded using a 1:1 solvent mixture of CH_2Cl_2 and methanol, while **B1**−**B5** data were recorded in CH_3NO_2. UV−vis spectra and excitation and emission spectra were recorded at room temperature. DSC measurements were carried out at a heating rate of 10°C/min under an argon atmosphere. TGA measurements were performed using a heating rate of 10°C/min under nitrogen. Cyclic voltammetry was measured in CH_2Cl_2 or DMF using 0.10 M $Bu_4N[PF_6]$ as the electrolyte. Ag/AgCl was used as the reference electrode, and a platinum electrode was used as the working electrode in a conventional three-compartment cell with ferrocene/ferrocenium ($FeCp_2/FeCp_2^+$) couple as the external standard. The scans toward the anodic and cathodic directions were performed separately at a scan rate of 100 and 500 mV/s, respectively, at room temperature. TLC was carried out on SiO_2. Column chromatography was carried out on silica. 8-Hydroxyquinoline, 8-hydroxy-2-methylquinoline, 1, 4-dibromobenzene, 4, 4′-dibromobiphenyl, 4-bromobenzonitrile, and 4-bromoacetophenone were purchased. 5-Bromo-8-methoxyquinoline and 5-bromo-8-methoxy-2-methylquinoline were prepared using previously reported procedures.[5,13] MOM ethers, 5-bromo-8-(methoxymethoxy)quinoline, and 5-bromo-8-(methoxymethoxy)-2-methylquinoline were prepared by alkylation of the corresponding alkoxide anions (deprotonated via NaH at 0 °C) with MOMCl in THF. All the boronic acids were prepared

according to modified literature procedures.[14] All the ligands **L1**/**L1′**−**L5**/**L5′** including intermediate 4-di(2-thienyl)benzene were synthesized using general Suzuki coupling procedures.[15]

Synthesis of 4, 4′-Di[5″-(8″-methoxyquinoline)]biphenyl (L1). 4,4′-Biphenyldiboronic acid (0.24 g, 1 mmol), 5-bromo-8-methoxyquinoline (0.545 g, 2.3 mmol), $Pd(PPh_3)_4$ (69 mg, 0.06 mmol), and Na_2CO_3 (0.50 g, 4.7 mmol) were added to a flask under nitrogen. A solvent mixture of toluene (45 mL), water (15 mL), and ethanol (15 mL) was degassed and added to the reaction mixture. The resulting mixture was refluxed with vigorous stirring for 18 h. After the mixture was cooled to room temperature, the organic phase and the aqueous phase were separated. The aqueous phase was extracted with CH_2Cl_2 (3 × 40 mL), and the extract was combined with the organic phase. After being dried over $MgSO_4$, the solvents were removed under reduced pressure. The residue was purified by column chromatography using THF/Hexane (4/1) as the eluent, and the subsequent recrystalization from hexane/CH_2Cl_2 afforded 0.37 g of **L1** as a white powder (yield 79%). ^{1}H NMR ($CDCl_3$, δ, ppm): 9.02 (1H, d, J = 3.8 Hz), 8.38 (1H, d, J = 8.5 Hz), 7.84 (2H, d, J = 7.78 Hz), 7.60 (2H, d, J = 7.8 Hz), 7.55 (1H, d, J = 7.9 Hz), 7.48 (1H, dd, J = 3.8 Hz, 8.5 Hz). 7.19 (1H, d, J = 8.0 Hz), 4.19 (3H, s). ^{13}C NMR ($CDCl_3$, δ, ppm): 154.8, 149.0, 139.7, 138.6, 134.6, 131.8, 130.7, 127.6, 127.5, 127.2, 121.7, 114.3, 107.3, 56.1. HRMS: calcd for $C_{32}H_{25}N_2O_2$ [M + H]$^+$, 469.1916; found, 469.1906.

The synthetic procedures and analytical data for **L2**−**L5** and **L0** are provided in the Supporting Information.

Syntheses of L1′−**L5′**. Molecules of **L1′**−**L5′** are analogues of **L1**−**L5** with the 8-methoxy group being replaced by a 8-methoxymethoxy (MOMO) on the quinoline ring. The synthetic procedures for **L1′**−**L5′** are identical as those used for **L1**−**L5** except that one of the starting materials, 5-bromo-8-methoxyquinoline, is replaced by 5-bromo-8-methoxymethoxyquinoline for **L1′** and **L3′**−**L5′**, and by 5-bromo-8-methoxymethoxy-2-methylquinoline for **L2′**. For details, please see the Supporting Information.

General Procedures for the Syntheses of L(OH)1−**L(OH)5.** **L1′**−**L5′** were dissolved in 30 mL of mixed solvents of MeOH and CH_2Cl_2 (2:1) as a suspension in a round-bottom flask equipped with a condenser. When 1 mL of concentrated HCl was slowly added, the reaction mixture immediately turned to a clear yellow solution. After it was refluxed for about 24 h, the yellow mixture became a suspension again from a clear solution. After it was cooled to room temperature, the mixture was neutralized with saturated $NaHCO_3$, and yellow-green precipitation was obtained. By washing with CH_2Cl_2 (3 × 20 mL), **L**(OH)**1**−**L**(OH)**5** were collected in excellent yields (85−92%) by filtration, which were used for cheleation with BPh_3 without further purification.

L(OH)1: Yield 91%. ^{1}H NMR (DMSO, δ, ppm): 10.00(1H, s), 8.93 (1H, d, J = 2.7 Hz), 8.33 (1H, d, J = 8.0 Hz), 7.92 (2H, d, J = 6.4 Hz), 7.62−7.59 (3H, m), 7.50 (1H, d, J = 8.0 Hz), 7.20-(1H, d, J = 8.0 Hz).

Data for **L**(OH)**2**−**L**(OH)**5** and **L**(OH)**0** are provided in the Supporting Information.

General Procedures for the Synthesis of Boron Complexes. THF solutions of 2 equiv of BPh_3 for **B1**, **B2**, and **B5** and 3 equiv for **B3** and **B4** were added to a stirred suspension of the corresponding ligands **L1**(OH)**1**−**L**(OH)**5** in THF. Each reaction mixture was refluxed. The initial suspension dissolved completely after the mixture was refluxed for over 24 h. After concentrating the solution by vacuum, the crude yellow-green powders of **B1**−**B4** or orange powder of **B5** was isolated and was further purified by recrystallization from CH_2Cl_2 and hexane.

Synthesis of 4,4′-Bis(Ph$_2$B-8″-hydroxyquinolate)biphenyl (B1). Following the general procedure for the syntheses of the boron complexes, the reaction between BPh_3 (123 mg, 0.51 mmol) and **L**(OH)**1** (106 mg, 0.24 mmol) in THF afforded the yellow-green powder of **B1** in 67% yield (123 mg, 0.16 mmol). ^{1}H NMR (CD_2Cl_2, δ, ppm): 8.69 (1H, d, J = 8.4 Hz), 8.67 (1H, d, J = 4.8 Hz), 7.86 (2H, d, J = 6.6 Hz), 7.77 (1H, d, J = 7.8), 7.71 (1H, dd, J = 4.8, 8.4 Hz), 7.64 (2H, d, J = 7.8 Hz), 7.47−7.45 (4H, m), 7.30−7.27 (7H, m). ^{13}C NMR (CD_2Cl_2, δ, ppm): 158.2, 139.7, 139.6, 138.0, 137.7, 137.4, 133.0, 131.9 (x2C), 130.1, 127.5 (x2C), 127.4, 126.90, 125.9, 123.2, 109.3. ^{11}B NMR (CD_2Cl_2, ppm): 11.2 ppm. HRMS: calcd for $C_{54}H_{38}B_2N_2O_2K$ [M + K]$^+$, 807.2768; found [M + K]$^+$, 807.2780.

The synthetic procedures for **B2**−**B5** and **B0** are provided in the Supporting Information.

X-ray Crystallography Analyses. Single-crystals of **L1**, **L3**, **L5**, and **B0** were obtained from CH_2Cl_2/hexane solution and were mounted on glass fibers in a brass pin. The data were collected on a single-crystal X-ray diffractometer with a detector and graphite-monochromated Mo Kα radiation operating at 50 kV and 30 mA at 25 °C, except for **L5** whose data were collected at −93 °C. No significant decay was observed during the data collection. Data were processed using the SHELXTL software package (version 5.10).[16] Neutral atom scattering factors were taken from Cromer and Waber.[17] Empirical absorption correction was applied to all crystals. The crystals of **L1** and **L3** belong to the triclinic space group $P\bar{1}$ while the crystals of **L5** and **B0** belong to the orthorhombic space group *Pbca* and the monoclinic space group $P2_1$, respectively. The structures were solved by direct methods. Disordered $CHCl_3$ solvent molecules were located in the crystal lattice of **L3**. Because of the difficulty in modeling the disordered solvent molecules in **L3**, their contributions were removed by using the SQUEEZE routine of the Platon software suite.[17b,17c] All non-hydrogen atoms except some of the disordered atoms were refined anisotropically. The positions of hydrogen atoms were calculated, and their contributions in structural factor calculations were included. Complete crystallographic data are provided in Supporting Information.

Quantum Yield Measurements. Quantum yields of compounds **B0**−**B5** and **L0**−**L5** were determined using either anthracene (Φ_r = 0.25) or 9,10-diphenylanthracene as the standard in CH_2Cl_2 at 298 K (Φ_r = 0.95).[18] The absorbance of all the samples and the standard at the excitation wavelength is approximately 0.098−0.109. The quantum yields were calculated using previously known procedures.[19] The absolute solid-state quantum efficiencies (SSQE) of luminescence were measured from freshly spin-coated films of chloroform solutions using an integrating sphere in terms of the previously reported procedures.[20]

Acknowledgment. We thank the Natural Sciences and Engineering Research Council of Canada for financial support. We are in debt to Dr. Jian-Ping Lu at the National Research Council for his assistance in recording the quantum yields in the solid state.

Supporting Information Available: Detailed experimental and synthetic procedures for all compounds reported here, complete crystal data for **L1**, **L3**, **L5**, and **B0** including tables of atomic coordinates, thermal parameters, bond lengths and angles, and hydrogen parameters, UV−vis data, NMR spectra, and TGA data, as well as Cartesian atom coordinates and absolute energies for ligands **L1**−**L5** obtained from Gaussian 98 calculations. This material is available free of charge via the Internet at http://pubs.acs.org.

JO060841+